Precision Radiometry and the APHID 22 GHz Water Line Monitor

A.I. Harris
Department of Astronomy, University of Maryland
May 3, 2000

BIMA Memo No. 80 (Also ALMA Memo No. 307)

Abstract

Fluctuating amounts of water vapor over an antenna in an interferometer add phase shifts to the instrument, shifting the fringe pattern on the sky to decrease signal correlation. Optically thin line radiation from the same water vapor that causes the decorrelation can be accurately measured, however, allowing an estimate of the column of water above individual antennas. Knowledge of the water column allows an equivalent but opposite phase to be inserted in the data processing; this is the radio equivalent of adaptive optics. This memo explores the instrumental requirements for a multi-channel radiometer capable of measuring pathlength differences to 35 μm, a goal for interferometry at 1 mm wavelength. An examination of linear and nonlinear error sources shows that residual amplifier or detector nonlinearity is likely to be the most significant instrumental limit for atmospheric phase correction.

1 Introduction

Variations in tropospheric water vapor introduce electrical pathlength changes through the atmosphere. Fluctuating pathlengths decrease signal correlation between elements of millimeter wave aperture synthesis arrays, degrading their sensitivity to astronomical signals. Increases in the water column produce not only a longer pathlength, but also stronger water vapor line emission; an observation of the integrated intensity of water line is a direct measure of the pathlength. APHID (Atmospheric PHase Inference Device) is a heterodyne spectrometer (multi-channel radiometer) optimized for precise measurements of the optically thin 22.235 GHz transition of water vapor. APHID's measurement goal is $\lambda/20$ for 1 mm wavelength observations, or 50 μm changes in pathlength. Allowing a factor $\sqrt{2}$ for combination of independent measurements for two antennas on an interferometric baseline, APHID's measurement accuracy at any one antenna must be 35 μm rms.

An absolute measurement of the total column of atmospheric water vapor with this precision is impossible at present, requiring more exact information of the line shape and atmospheric structure than is known or practically measurable. Differential pathlength measurements are nearly as useful for correcting millimeter-wave phases, however, and are much less sensitive to the details of atmospheric lineshapes.

Model calculations indicate that a 35 μm pathlength change corresponds to a 6×10^{-5} fractional change in the water line's integrated intensity [1]–[2] under typical conditions: a 20 K peak line temperature, 80 K receiver temperature, and a 400–4000 MHz spectrometer bandwidth with the line folded about its center. If APHID is to correct phases by absolute measurements alone, its measurement accuracy goal is consequently 1×10^{-5}, a few times better than the accuracy necessary for typical measurements. Demands on measurement precision can be reduced with frequent recalibration of the phase relationship to line temperature, which

replace absolute precision measurements with lower accuracy relative and empirically calibrated measurements.

In either case, the degree of accuracy is considerably higher than is necessary for typical astronomical radiometry, with the exception of Cosmic Microwave Background instruments. Astronomical radiometers extract very small signals from large backgrounds, but uncertainties in the astronomical signal's absolute scaling of several percent are often permissible. In addition, since APHID uses spectral information to separate the water line from antenna spillover and atmospheric quasi-continuum components, its demands on spectral fidelity are also extremely high.

The primary purpose of this note is to explore the instrumental requirements for radiometry with this degree of accuracy. If the system cannot be internally calibrated to this degree, it is still possible to calibrate against astronomically-derived phases; in this case, results in this note are useful for determining the range of operating conditions that still allow the necessary accuracy.

1.1 Precision Radiometry

An ideal radiometer would measure spectra with a perfectly constant conversion factor between a spectral channel's input noise temperature and its output voltage. In a real radiometer, even one which is perfectly linear, calibration load temperatures drift, optical standing waves change the coupling between loads and the radiometer input, power measurements have a certain accuracy, and the system's gain drifts with small changes in temperature or device bias conditions. Establishing APHID's sensitivity to these effects is the topic of Section 2.

All real radiometers are also nonlinear at some level, with some gain dependence on input power level, temperature, bias voltage, or other environmental parameters. Although temperatures and voltages can be carefully stabilized, the radiometer itself must be insensitive to changes in input power, since that must be permitted to vary. Changes in signal power shift the operating conditions of amplifiers, detectors, and other components, causing gain saturation at some level. Saturation causes errors by reducing the measured power below its true value and by adding spectral distortions. Section 3 explores the effects of changing input power level for a multi-channel radiometer with a nonlinear relationship between its input and output power levels.

1.2 Signal Combinations

APHID measures the following powers (after conversion from correlator lag voltages) on the sky, hot load, and cold load:

$$s_s = k(T_s + T_{rec})BG \quad (1)$$

$$s_h = k(T_h + T_{rec})BG \quad (2)$$

$$s_c = k(T_c + T_{rec})BG \quad (3)$$

where k is Boltzmann's constant, B is the channel bandwidth, G is the system's power gain; and T_s is the power from the sky, T_h and T_c are the hot and cold calibration load radiation temperatures, and T_{rec} is the radiometer's noise temperature referred to its input. T_s, T_h, and T_c are observed and may have additional contributions from, for instance, spillover. All of the temperature terms and the gains G in equations (1)–(3) will be frequency dependent, and G may have some dependence on input power level.

2 Errors for a Linear Radiometer

Assuming that the system gain is constant with value G_{cal} during the calibration, and has value G_{obs} during observations, solving equations (1)–(3) for T_s yields:

$$T_s = \frac{(gs_s - s_c)T_h - (gs_s - s_h)T_c}{s_h - s_c} \tag{4}$$

for the absolute temperature in a given spectral channel, where the gain ratio $g = G_{cal}/G_{obs}$. Using equation (4), the difference between two sky measurements using the same load calibration is:

$$\delta T_s \equiv T_{sky,1} - T_{sky,2} = \frac{T_h - T_c}{s_h - s_c}\left(g_1\, s_{s,1} - g_2\, s_{s,2}\right) . \tag{5}$$

Errors in difference measurements will depend on errors in power, gain, and temperature. These enter the conversion factor $K_\delta = \delta T_s/\delta s_s$ anew at each calibration cycle. Some simplification is possible when the gain is stable during the measurements, so $g_1 = g_2 \equiv g$, but saturation or other effects change the gain between calibration and observations (see sec. 3). In this case,

$$\delta T_s = K_\delta(s_{s,1} - s_{s,2}) , \tag{6}$$

with the gain factor

$$K_\delta = \frac{T_h - T_c}{s_h - s_c}\, g . \tag{7}$$

This expression also gives a good estimate of the difference signals' general sensitivity to gain variation.

2.1 Error Sensitivity

2.1.1 Absolute Measurements

Differentiating equation (4) gives the linearized sensitivity to small errors in its component parts. For errors in T_h, the change in T_s normalized to the calibration difference, $\Delta T_{cal} = T_h - T_c$, is:

$$\frac{\Delta T_s}{\Delta T_{cal}} \approx \frac{1}{\Delta T_{cal}}\frac{\partial T_s}{\partial T_h}\,\Delta T_h = \frac{gs_s - s_c}{s_h - s_c}\,\frac{\Delta T_h}{\Delta T_{cal}} , \tag{8}$$

with errors in T_c,

$$\frac{\Delta T_s}{\Delta T_{cal}} \approx \frac{1}{\Delta T_{cal}}\frac{\partial T_s}{\partial T_c}\,\Delta T_c = -\frac{gs_s - s_h}{s_h - s_c}\,\frac{\Delta T_c}{\Delta T_{cal}} . \tag{9}$$

For errors in s_h,

$$\frac{\Delta T_s}{\Delta T_{cal}} \approx \frac{1}{\Delta T_{cal}}\frac{\partial T_s}{\partial s_h}\,\Delta s_h = -\frac{(gs_s - s_c)s_h}{(s_h - s_c)^2}\,\frac{\Delta s_h}{s_h} , \tag{10}$$

errors in s_c,

$$\frac{\Delta T_s}{\Delta T_{cal}} \approx \frac{1}{\Delta T_{cal}}\frac{\partial T_s}{\partial s_c}\,\Delta s_c = \frac{(gs_s - s_h)s_c}{(s_h - s_c)^2}\,\frac{\Delta s_c}{s_c} , \tag{11}$$

and errors in s_s,

$$\frac{\Delta T_s}{\Delta T_{cal}} \approx \frac{1}{\Delta T_{cal}}\frac{\partial T_s}{\partial s_s}\,\Delta s_s = \frac{gs_s}{s_h - s_c}\,\frac{\Delta s_s}{s_s} . \tag{12}$$

Errors in the normalized gain factor $g = G_{cal}/G_{obs}$ enter as:

$$\frac{\Delta T_s}{\Delta T_{cal}} \approx \frac{1}{\Delta T_{cal}}\frac{\partial T_s}{\partial g}\,\Delta g = \frac{gs_s}{s_h - s_c}\,\frac{\Delta g}{g} . \tag{13}$$

2.1.2 Difference Measurements

Differentiating K_δ and dividing by K_δ (eq. 7) gives the linearized fractional error sensitivity for differential sky measurements:

$$\frac{\Delta K_\delta}{K_\delta} \approx \frac{1}{K_\delta}\frac{\partial K_\delta}{\partial T_h}\,\Delta T_h = \frac{\Delta T_h}{\Delta T_{cal}}\;; \tag{14}$$

the sensitivity to T_c is the same but has the opposite sign. For errors in s_h,

$$\frac{\Delta K_\delta}{K_\delta} \approx \frac{1}{K_\delta}\frac{\partial K_\delta}{\partial s_h}\,\Delta s_h = -\frac{g s_h}{s_h - s_c}\,\frac{\Delta s_h}{s_h}\,, \tag{15}$$

and for s_c,

$$\frac{\Delta K_\delta}{K_\delta} \approx \frac{1}{K_\delta}\frac{\partial K_\delta}{\partial s_c}\,\Delta s_c = \frac{g s_c}{s_h - s_c}\,\frac{\Delta s_c}{s_c}\,. \tag{16}$$

The sensitivity to gain variations between two observations or an observation and calibration is:

$$\frac{\Delta K_\delta}{K_\delta} \approx \frac{1}{K_\delta}\frac{\partial K_\delta}{\partial g}\,\Delta g = \frac{\Delta g}{g}\,. \tag{17}$$

2.2 Representative Requirements

2.2.1 Absolute Measurements

In some cases an absolute measurement is required, but one with relaxed accuracy. For instance, an uncertainty of $\Delta T_s = 100$ mK may well be adequate for finding the approximate total water vapor column. In this case, equations (8)–(13) set limits on load and measurement uncertainties. As a concrete example, take $\Delta T_s = 100$ mK and APHID's typical operating conditions of $T_s \approx 100$ K, $T_h \approx 300$ K, and $T_c \approx 80$ K. Letting $g = 1$ and choosing an (arbitrary) scale factor that produces corresponding powers of $s_s = 100$ W, $s_h = 300$ W, and $s_c = 80$ W, equations (8)–(13) yield individual limits of $\Delta T_h < 1.1$ K, $\Delta T_c < 110$ mK, $\Delta s_h/s_h < 3.7 \times 10^{-3}$, $\Delta s_c/s_c < 1.4 \times 10^{-3}$, and $\Delta s_s/s_s < 1.0 \times 10^{-3}$. Fractional temperature error of a part in 10^3 requires a fractional gain stability of 1.0×10^{-3} for this set of assumptions. If all of the errors are present and uncorrelated, then this "error budget" for each should be divided by approximately the square root of the number of independent terms, or $\sqrt{6} = 2.45$. For typical integration times, temperature and gain errors dominate, so a factor of 1.5–2 is more realistic (also see sec. 2.3).

The practical limit on load temperature knowledge is likely to be in the optical path rather than in the thermometry. Apertures, windows, and other elements have frequency-dependent transmission and emission from beam truncation and scattering. This can make it difficult to relate measurements of the load's physical temperature to its radiation temperature.

2.2.2 Difference Measurements

Estimates for differential measurements follow a similar logic, but now for the conversion factor. A fractional measurement accuracy of 10^{-5} requires $|\Delta K_\delta|/K_\delta < 10^{-5}$. Using the powers and temperatures from sec. 2.2.1, equations (14)–(17) indicate calibration with reproducibility (but not absolute accuracy) of $\Delta T_h = \Delta T_c < 2.2$ mK, $\Delta s_h/s_h < 7.3 \times 10^{-6}$, $\Delta s_c/s_c < 2.8 \times 10^{-5}$, and $\Delta g/g < 10^{-5}$.

2.3 *Measurement Time*

A given fractional power accuracy requirement in the spectrum determines the minimum integration time τ through the radiometer equation,

$$\frac{\Delta s}{s} = \frac{1}{\sqrt{B\tau}} \,, \tag{18}$$

where B is the bandwidth of the channel in the spectrum. For $\Delta s/s = 5 \times 10^{-6}$ and $B =$ 3.5 GHz, $\tau = 88$ ms, much shorter than the typical integration times. Measurement time should not limit the measurement accuracy for calibration.

3 Errors for a Nonlinear Radiometer

3.1 *Saturation or Gain Compression*

Gain saturation (or compression) can be generally modeled by a polynomial in power ($v_{out} = \alpha_0 + \alpha_1 P_{in} + \alpha_2 P_{in}^2 + \cdots$) or a number of analytical approximations. A power law fit is very accurate over the range of input data but has no simple form for investigating the general properties of saturation. A hyperbolic tangent $\tanh(s)$ function is not necessarily exact, but is a useful and tractable approximation for the saturation behavior of many devices.

Figures 1 and 2 show that a $\tanh(s)$ behavior is a very good working approximation to the saturation law for the Gilbert-cell analog multipliers in the APHID spectrometer and microwave amplifiers at low power levels. The $\tanh(s)$ compression law is expected theoretically for simple Gilbert cells [4]–[5], although a variety of effects and embedding circuits can change this characteristic [4]. Figure 1 is laboratory confirmation that the Gilbert cell devices in APHID do not have predistortion circuits, and that they follow a clean $\tanh(s)$ law. The dashed line in the figure shows an ideal linear behavior; the ratio of the linear curve to the measured points is the gain compression factor.

Devices with feedback will operate linearly over a wider range of low power inputs than a $\tanh(s)$ approximation would indicate, but will saturate in a generally similar way. If the gain per stage with feedback is not large, as is often the case for microwave amplifiers, feedback's effect on transistor nonlinearity may not be very large. Figure 2 summarizes measurements of power saturation with a broadband noise input measurements a typical power amplifiers [3]–[7]. A $\tanh(s)$ fit works well for modest compression, but then slowly fails as the output power compression increases, quite possibly because the dominant nature of the nonlinearity changes from transistor gain to bias constraints. This measurement shows that a $\tanh(s)$ approximation is quite useful for understanding the general effects of low-level saturation and for making quantitative estimates of system performance.

3.1.1 Absolute and differential gain and compression

The output signal from a device with a hyperbolic tangent relationship between input and output signals s_i and s_o is

$$s_o = G_A \, a \, \tanh\left(\frac{s_i}{a}\right) \,, \tag{19}$$

where G_A is an overall linear gain factor and a is the asymptotic saturation value referred to the input. For $s_i \ll a$, the expansion $\tanh(x) = x - x^3/3 + \cdots$ shows that this expression properly reduces to the ideal linear case, $s_o = G_A \, s_i$. The absolute gain compression factor f_A

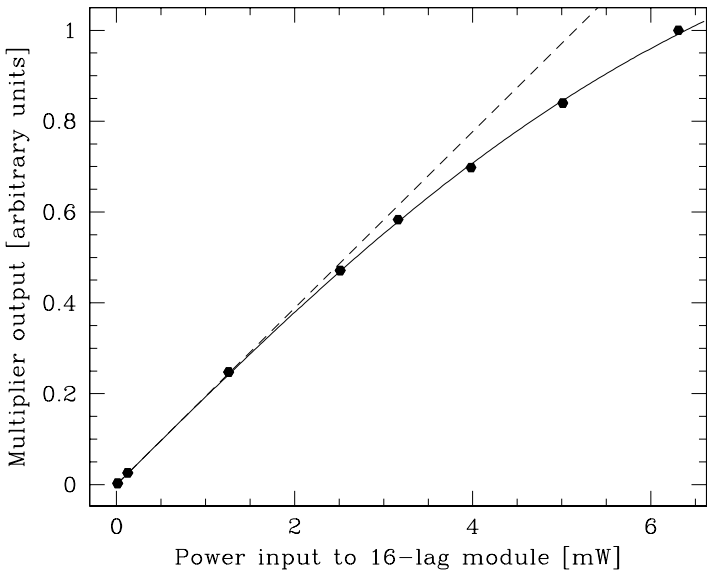

Figure 1: Compression curve for APHID's multiplier modules at a sample frequency of 1.2 GHz (points) and a least-square fit with a $\tanh(s)$ function. The dashed line is a perfectly linear response. The fitted value for the saturation factor a is 7.3 mW at the module's input.

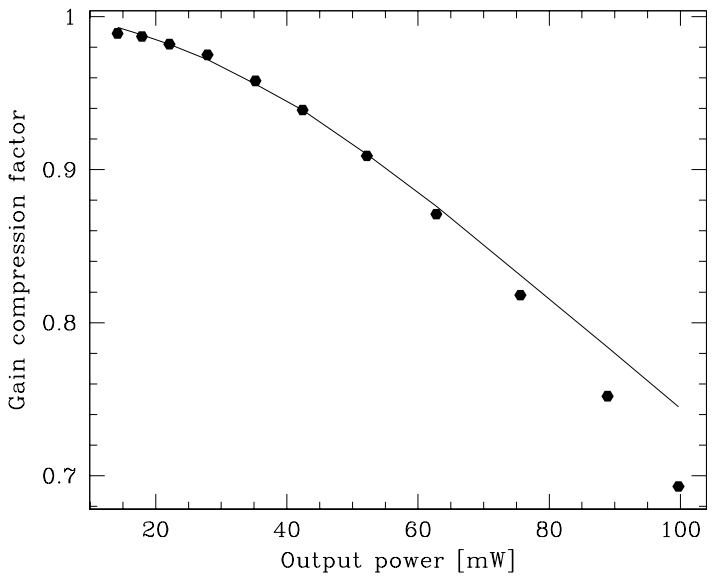

Figure 2: Measured gain compression factor with broadband noise (points) and an unconstrained plot of a $a/s_i \tanh(s_i/a)$ function fixed to the point at a compression near 0.5 dB.

is the gain ratio between the compressed and ideal linear systems:

$$f_A = \frac{s_o(compr)}{s_o(ideal)} = \frac{a}{s_i} \tanh\left(\frac{s_i}{a}\right) \tag{20}$$

as a function of the ratio of input to saturation values, s_i and a. The 1 dB compression point occurs at $s_i/a = 0.905$; for 0.5 dB compression, $s_i/a = 0.612$.

Essentially all astronomical measurements are differences between two signals. Common differences are between on and off source positions, or hot and cold calibration loads. In some cases (e.g. switching between on and off source positions) the difference signal is miniscule. The comparatively large background signal affects the radiometer by establishing its average operating point. In other cases (e.g. passband gain calibration) the signals themselves considerably shift the operating point between measurements. From equation (20) the ratio of compressed to ideal difference outputs for arbitrary input levels is:

$$f_\Delta = \frac{\Delta s_o(compr)}{\Delta s_o(ideal)} = \frac{a\left[\tanh\left(s_{i1}/a\right) - \tanh\left(s_{i2}/a\right)\right]}{s_{i1} - s_{i2}} \,. \tag{21}$$

For instrument design, when a domain but not the exact operating conditions are known, the limiting cases of equation (21) are useful. In the large differential signal limit, one signal is much larger than the other, $s_{i1} \gg s_{i2}$, and the gain compression factor is given by equation (20) with $s_i = s_{i1}$. In the small differential signal limit, $s_{i1} \approx s_{i2}$, and the difference Δs_i tends to zero around an average operating point s_i,

$$\Delta s_o \approx \frac{d}{ds}\left[G_A\, a\, \tanh\left(\frac{s}{a}\right)\right]_{s_i} \Delta s_i = G_A \operatorname{sech}^2\left(\frac{s_i}{a}\right) \Delta s_i \,. \tag{22}$$

Combining this expansion with an ideal linear system's $\Delta s_o = G_A\, \Delta s_i$ and the identity $\operatorname{sech}^2(x) = 1 - \tanh^2(x)$ yields:

$$f_{\Delta,diffl} = 1 - \tanh^2\left(\frac{s_i}{a}\right) \,. \tag{23}$$

Equation (23) is the more stringent limit on the gain compression factor.

It may seem odd that changes in the gain compression factor is larger for small differential signals than for large-scale signal swings. The reason for this is that large-signal case describes a single signal which retains most of its amplitude, while the small-signal differential limit is very sensitive to the local slope of the curve that describes the saturation.

A direct solution involves examining how saturation changes the gain ratio g as the input power increases by amount Δs from s_i. The gain ratio in this situation is:

$$g = \frac{G(s_i + \Delta s)}{G(s_i)} = \frac{1}{1+y} \frac{\tanh\left[x\,(1+y)\right]}{\tanh\left(x\right)} \,, \tag{24}$$

where $x = s_i/a$ and $y = \Delta s/s_i$. There is no closed-form solution to the factor y in equation (24); Figure 4 shows the numerical solution. For a device operating 10 dB below its 1 dB compression point, for instance, a fractional gain change below 10^{-5} implies a maximum signal shift of about 27 dB below the input power level, or a 0.2 K shift for a 100 K system temperature.

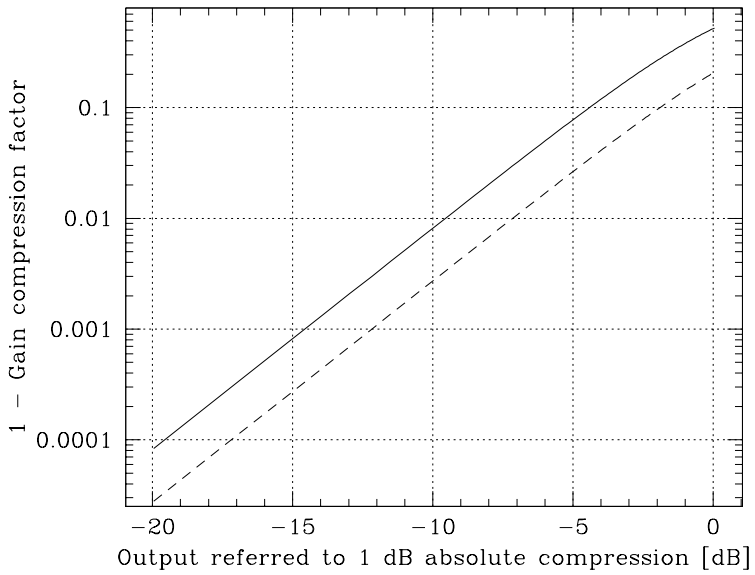

Figure 3: Gain compression factor defect limits versus output level for a device with a $\tanh(s)$ nonlinearity. The solid curve is for small differences, the dashed curve is for large signal changes.

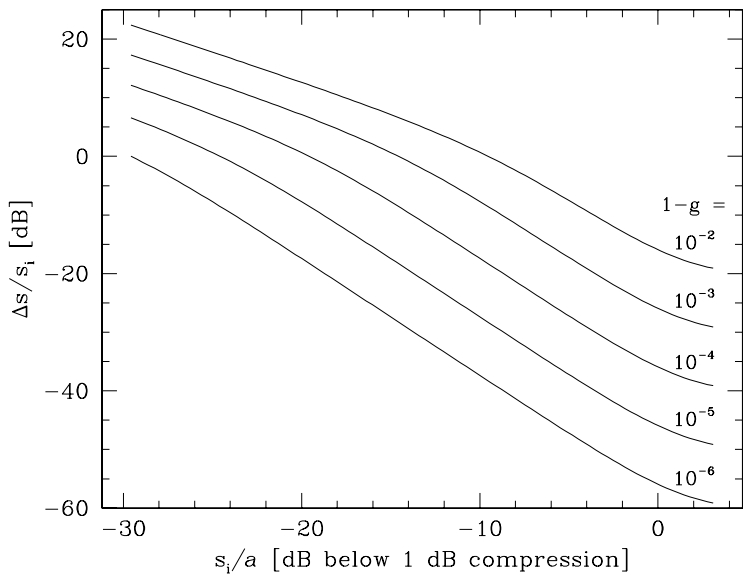

Figure 4: Gain compression error from equation (24) as a function of input signal level. Each curve represents a different gain error.

3.2 Calibration dynamic range

A common calibration problem is minor amplifier gain saturation during measurements of loads with temperatures well above the sky temperature. The system gain (passband) derived from this measurement will be artificially low at frequencies where the amplifier has saturated slightly, typically at frequencies where the system gain is highest. When applied to measured signals as a passband correction, these incorrect gains will distort the spectrum, even if the power level for sky measurements is low enough to avoid saturation.

Calibrating one spectrum by dividing by another will introduce an additional gain error. Dividing an atmospheric spectrum by a blackbody spectrum measured with a maximum power at 10 dB below the 1 dB point introduces almost a 1% error in the atmospheric scale. Unlike uncertainties that come from changing amounts of sky power, however, these error sources are stable (for the stable load temperatures) and can be removed by an initial calibration, at least to some degree.

3.3 Direct differential gain measurement

It is possible to measure the radiometer's differential gain directly by injecting and synchronously detecting a small amount of modulated noise. The radiometer equation links the length of time t_{mod} necessary to measure the modulated noise, compared with the time t_{sky} needed to integrate the sky signal to a given rms σ, as:

$$\frac{t_{mod}}{t_{sky}} = 2\left(\frac{\sigma}{p\,\Delta T_m}\right)^2 , \tag{25}$$

where p is the necessary accuracy, ΔT_m is the amount of modulated noise, and the factor two accounts for error propagation in the two independent measurements of ΔT_m. For instance, if $\sigma = 1$ mK and $\Delta T_m = 2$ K, measuring the system gain with a fractional accuracy $p = 10^{-5}$ requires an integration 5000 times longer than the sky signal integration. The magnitude of the maximum allowable noise modulation is given by equation (24) (Figure 4).

3.4 Device Effects

3.4.1 Amplifiers

Amplifiers can introduce spectral shape as well as overall gain reduction as they saturate. Saturation occurs for a given output power level, and spectral distortion and structure arises for a given input power level at frequencies of maximum gain, with decreasing saturation levels at frequencies where the gain is lower. Signals outside the amplifier's nominal passband sometimes also cause saturation.

Compression is usually measured with a coherent signal, which sets an upper limit for broadband noise inputs. Broadband noise combines with amplifier nonlinearity to generate intermodulation products throughout the band. This causes saturation for a broadband input signal even when its average power is the same as a coherent source's. Measurement of saturation in the WASP microwave amplifiers [6]–[7] shows that the amplifier saturates in the same way for noise and coherent signals, but with the noise saturation curve shifted to an output noise power 1.5 dB below the coherent signals'.

To minimize saturation effects, the usual rule of thumb for amplifiers is to operate at a maximum power level about 10 dB below the 1 dB absolute gain compression point. Figure 3 indicates that operation at this power level causes calibration errors of about 1%, which is

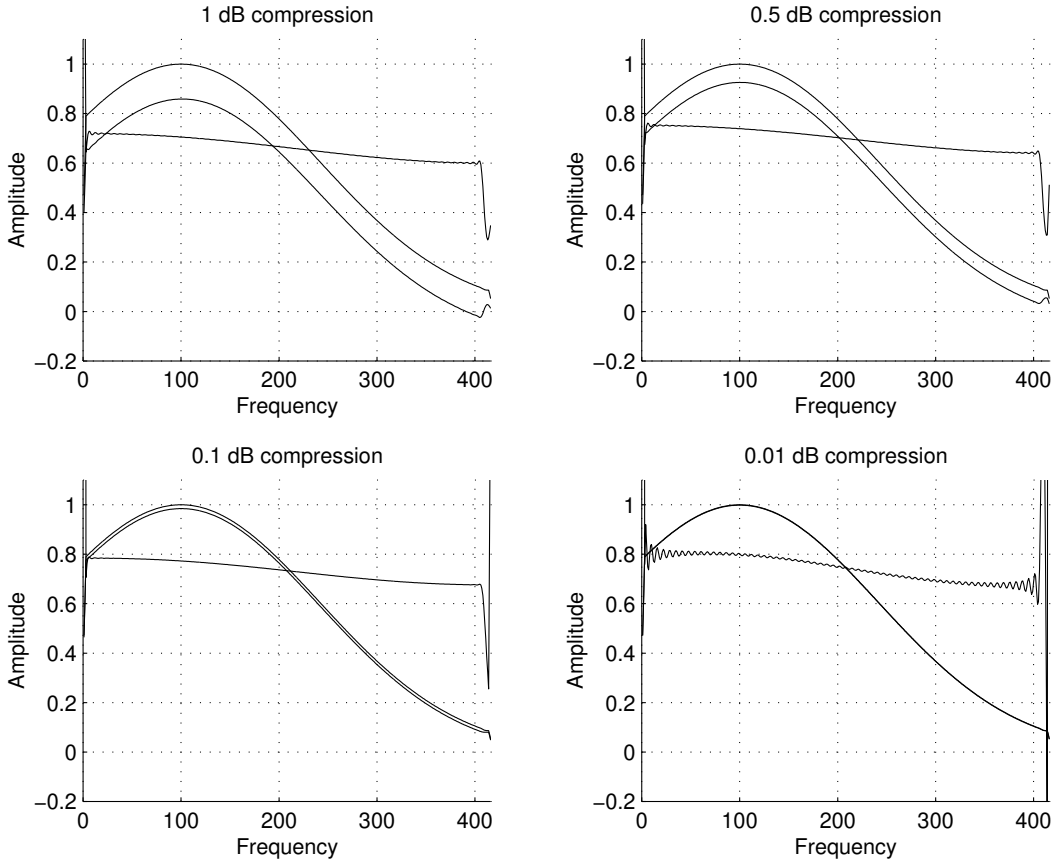

Figure 5: Compression in correlator multipliers for an input signal with a smooth bandpass. The upper curve in each frame is the input spectrum, the similar curve slightly below is the spectrum with a $\tanh(x)$ compression, and the slightly tilted line below is the difference between the two magnified by factors of 5, 10, 50, and 500 in panels with decreasing compression.

acceptable for many applications if not for APHID. For APHID in the absence of active gain measurement, values from Figure 3 and the additional 1.5 dB margin for broadband noise suggests that the signal level should be 22 dB below the coherent signal 1 dB compression point.

3.4.2 Autocorrelation spectrometers

Autocorrelation spectrometers shift and distort the spectrum as their multipliers saturate. The effect of multiplier saturation is different than amplifier saturation, which to first order simply scales the entire spectrum. Figure 5 is a MATLAB model result for the WASP 128-lag analog correlator spectrometer [3], showing the saturation effects over a range of compression levels. Each input spectrum was transformed to the time (lag) domain, multiplied by an $a\tanh(x/a)$ saturation term (equation (19)) with a common saturation factor a determined from the saturation level and peak value of all lags, and then transformed back into the spectral domain. Figure 5's panels show these input and output spectra and the difference between them.

Compared with the input spectra, the output spectra have both an overall shift in total power and a roughly cosine shaped structure across the passband (the plots also contain edge effects that are artifacts of smoothing near the band edges). These spectral distortions are

easy to understand qualitatively: the zero time lag, measuring total power, has the highest amplitude and saturates most strongly. Subsequent lags, containing information on line shape, have lower amplitudes and saturate less. Since the shape of the distortion depends on the input level in a nonlinear manner, it changes somewhat with saturation level. The distortion also changes with input spectrum because the lag voltages are distributed differently. In both cases, synchronous detection of a small modulated noise signal can provide a good channel-by-channel estimate of each lag's saturation.

3.4.3 Power Detectors

A typical power detector has a simple relationship between between input power P_{in} and output voltage v_{out},

$$v_{out} = R \left(\frac{P_{in}}{P_o} \right)^{\alpha} + v_{off} \ , \tag{26}$$

where R is a scaling constant in volts at a reference power level P_o. An ideal detector has $\alpha = 1$ and $v_{off} = 0$; deviations from these are nonlinear errors. The power law coefficient α can be tuned close to unity over a reasonable power range by changing the impedance of the circuit following the detector. For $v_{off} = 0$, a mistuning in the circuit causes a scaling error of $(P_{in}/P_o)^{\alpha-1}$, which may be important depending on the necessary accuracy, the value of α, and the difference in power from the reference level. APHID does not depend on precise power detectors of this sort, but filter bank or digital correlator spectrometers rely on linear power detectors.

3.4.4 Analog to Digital Converters

Depending on construction, analog to digital converters (ADCs) can introduce significant nonlinearity. Averaging over many noise samples with rms of at least a least significant bit (LSB) yields average values with precision better than a LSB, so the important specification is deviation from nominal linearity. Successive-approximation or flash converters can deviate from linearity by up to one half least significant bit (LSB), although they are often better for modest numbers of bits. Charge-balancing converters, for instance dual slope or Δ–Σ, are slower but have substantially better specifications on linearity. The manufacturer of APHID's ADCs [8] specifies a maximum integral nonlinearity of $\pm 0.024\%$ of full scale range for a full-scale signal. The linearity is better for smaller signals. In APHID's case, ADC linearity enters in the same way as autocorrelator multiplier linearity, affecting the lags with higher signal levels more strongly than the lags with lower signal levels.

4 Conclusion

Meeting APHID's measurement goal for phase correction by requiring a raw instrumental fractional precision of 10^{-5} under all conditions will be extremely difficult. Measuring an amplitude-modulated noise signal injected at the radiometer's input seems to be necessary to compensate for residual amplifier, spectrometer, and ADC nonlinearity. The time necessary for the measurement may not be short compared with the time over which the entire system drifts, however. Temperature measurement resolution of 1 mK is necessary for the calibration black-body loads but is a secondary problem.

A fractional accuracy of 10^{-4} is a more reasonable goal, however. Correcting the interferometer maps will still be possible but will require a tight interplay between radiometer calibration and measurements of the millimeter-wave phases: the "kelvins per radians" at the spectrometer

output will not be a constant, but will need to be empirically recalibrated as the weather or source altitude change. With a frequent and empirical calibration, very optically thin lines have no fundamental advantage over lines with moderate depth for phase recovery. The choice of line will come to tradeoffs between line intensity and the separation of water vapor emission from continuum and atmospheric quasi-continuum contributions.

Acknowledgments

I thank David Woody, Jonhannes Staguhn, Jack Welch, and Lee Mundy for their insights and useful comments. Work on water line radiometry at the University of Maryland receives support from National Radio Astronomy Observatory ALMA development funds through the MDC, NSF support of the BIMA consortium through grant AST99-81289, and the State of Maryland.

References

[1] Staguhn, J., Harris, A.I., Plambeck, R.L. & Welch, W.J. 1998, *Proc. SPIE* 3357, 432–441 (1998).

[2] ATM, a programming environment for atmospheric modeling. Mundy, L.G., Staguhn, J. & Teuben, P.

[3] Harris, A.I., Isaak, K.G. & Zmuidzinas, J., *Proc. SPIE* 3357, 384–394 (1998).

[4] Gilbert, B., IEEE SC-3, 365–373 (1968).

[5] Gray, P.R. & Meyer, R.G., *Analysis and Design of Analog Integrated Circuits*, ch. 10.3, John Wiley & Sons, N.Y. (1977).

[6] DBS Amplifier model DBS96-0058, with 36 dB gain, 1 dB compression at +23 dBm, IP2 and IP3 unknown.

[7] The compression measurement for broadband noise was made by increasing input power to the amplifier while monitoring its gain, relative to gain with no additional input signal, with a weak probe signal from an HP8720D network analyzer. The probe signal power was more than 10 dB below a power level which caused any amplifier gain compression. The probe signal was injected into the amplifier's input with a power combiner at the amplifier input; broadband noise from a noise diode and amplifier chain was injected through the other port. The amplifier's output power was measured with a power meter on a directional coupler at the output.

[8] Burr-Brown charge-integrating analog-to-digital converter model DDC101U.